Geophys. J. Int. (2008) **175,** 222–238 doi: 10.1111/j.1365-246X.2008.03887.x

Source inversion of W phase: speeding up seismic tsunami warning

Hiroo Kanamori[1] and Luis Rivera[2]

[1] *Seismological Lab., California Inst. of Technology, Pasadena, CA USA. E-mail: hiroo@gps.caltech.edu*
[2] *Institut de Physique du Globe de Strasbourg, CNRS-ULP,* 5 *rue René Descartes, Strasbourg Cedex,* 67084 *France*

Accepted 2008 June 12. Received 2008 June 12; in original form 2008 April 2

SUMMARY

W phase is a long period phase arriving before *S* wave. It can be interpreted as superposition of the fundamental, first, second and third overtones of spheroidal modes or Rayleigh waves and has a group velocity from 4.5 to 9 km s^{-1} over a period range of 100–1000 s. The amplitude of long period waves better represents the tsunami potential of an earthquake. Because of the fast group velocity of W phase, most of W phase energy is contained within a short time window after the arrival of the *P* wave. At a distance of 50°, W phase energy is contained within 23 min after the origin time which is the distinct advantage of using W phase for rapid tsunami warning purposes. We use a time domain deconvolution method to extract W phases from the broad-band records of global seismic networks. The bandwidth of W phase is approximately from 0.001 to 0.01 Hz, and we bandpass filter the data from 0.001 to 0.005 Hz in most cases. Having extracted W phase from the vertical component records, we perform a linear inversion using a point source to determine M_w and the source mechanism for several large earthquakes including the 2004 Sumatra–Andaman earthquake, the 2005 Nias earthquake, the 2006 Kuril Is. earthquake and the 2007 Sumatra earthquake. W phase inversion yields reliable solutions and holds promise of the use of W phase for rapid assessment of tsunami potential.

Key words: Tsunamis; Earthquake source observations; Surface waves and free oscillations; Wave propagation, Early warning.

1 INTRODUCTION

The 2004 Sumatra–Andaman Is. Earthquake ($M_w = 9.2$) excited Indian ocean wide tsunamis and caused widespread damage with an unprecedented magnitude with more than 283 000 casualties. This event motivated a renewed interest in developing effective tsunami warning systems which can help mitigate tragic tsunami damage in the future. Effective tsunami warning must have at least four elements: (1) detection of events, usually earthquakes, (2) detection of tsunami, (3) infrastructure for tsunami warning and (4) education and training of the public. In recent years, many new methodologies have been developed for detecting earthquakes and tsunamis using seismic networks, pressure gauges and GPS (e.g. recent reviews by Satake 2007; Hirshorn & Weinstein 2008). We call the basic tsunami warning method using seismic data collected from regional and global seismic networks the seismic tsunami warning method.

The seismic tsunami warning method does not directly measure tsunamis; instead it estimates the tsunamigenic potential of an earthquake from the seismic parameters such as the location, magnitude and mechanism. In this sense, it is indirect and is prone to false alarms. Nevertheless, it has a long history and is still one of the most basic elements of tsunami warning as is practiced by the Pacific Tsunami Warning Center in Hawaii, Japan Meteorological Agency in Japan and several others. It has a distinct advantage of being able to use the existing seismic stations deployed and maintained for general earthquake research and monitoring. Also, since seismograms can be used in many different ways, seismic warning methods can be made very versatile. In view of the recent extensive deployments of modern global seismic stations, we can now significantly improve the seismic warning method with introduction of novel concepts and methodology. In this paper, we use seismic W phase which carries long period information of the source at a much faster speed than the traditional surface waves. This wave has not been utilized because its suitability for rapid warning purposes has not been fully recognized. We will show that W phases can be retrieved on the time domain and used for rapid and robust determination of seismic source parameters with sufficient accuracy for tsunami warning purposes, especially for great earthquakes and slow tsunami earthquakes for which the traditional methods are not always effective. In particular, we aim at developing a method which can recognize a truly great earthquake like the 2004 Sumatra–Andaman Is. earthquake with the potential of widespread tsunami hazard. Also, we aim at a warning time (time between the earthquake origin time and the issuance of warning) of about 30 min, because the tsunami arrival times to near sites from damaging tsunami earthquakes such as the 1896 Sanriku earthquake and the 2006 Java earthquake range from 30 min to 1 hr.

2 W PHASE

The W phase is a distinct long-period, up to 1000 s, phase which arrives before S phase (Fig. 1). It was observed on the displacement

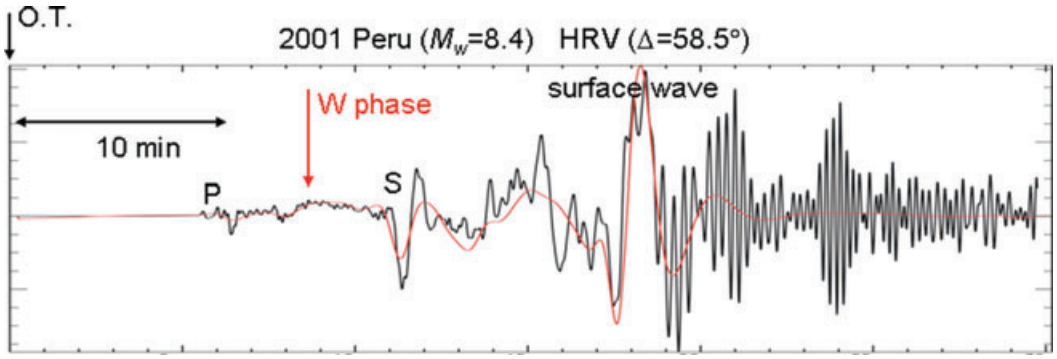

Figure 1. W phase from the 2001 Peruvian earthquake ($M_w = 8.4$) recorded at HRV, and the synthetic W phase computed by mode summation using the GCMT solution.

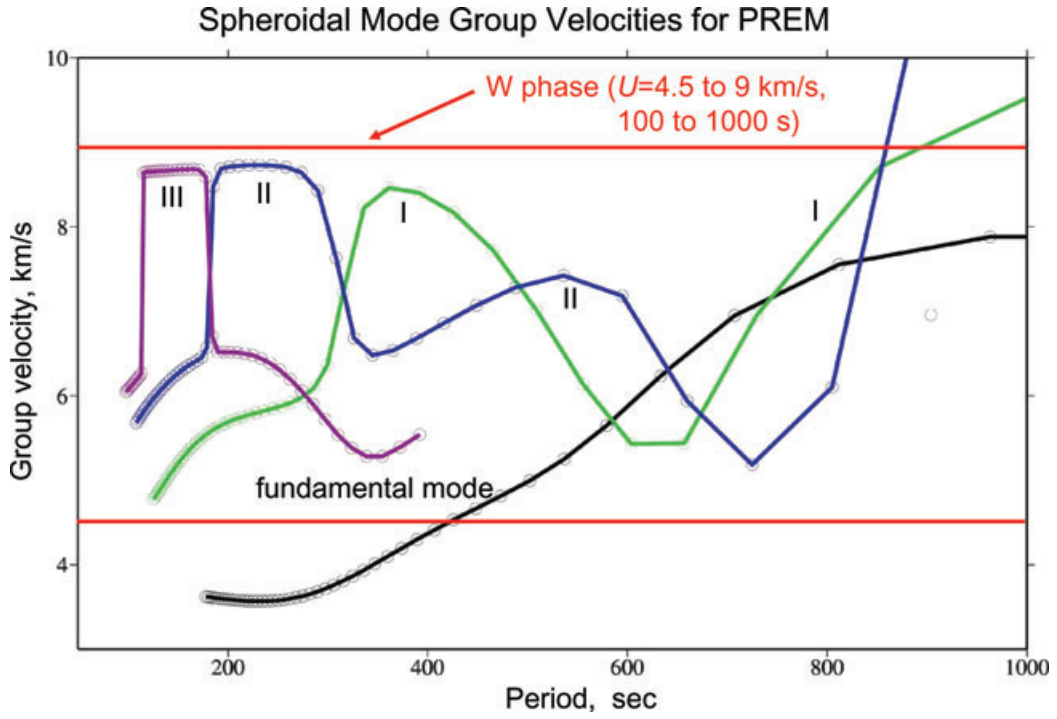

Figure 2. Group velocity dispersion curves of spheroidal modes computed for PREM. Dispersion curves for the fundamental mode (black), the first overtone (green), the second overtone (blue) and the third overtone (magenta) are shown. The horizontal red lines bound the group velocity of W phase.

records of the 1992 Nicaragua tsunami earthquake and, because of its distinct waveform, it was given a name W phase (Kanamori 1993). Theoretically, it represents the total, both near- and far-field, long-period wave-field from the source. In terms of seismic ray theory, it can also be interpreted as superposition of long-period energy associated with several phases such as P, PP, SP and S. In normal mode theory, W phase can be interpreted as superposition of the fundamental mode, first, second and third overtones of spheroidal modes at long period (i.e. Rayleigh waves) indicated by the two horizontal red lines in Fig. 2 which displays the group velocity dispersion curves of these modes computed for the Preliminary Reference Earth Model (PREM, Dziewonski & Anderson 1981). The group velocity of W phase ranges from 4.5 to 9 km s^{-1} over a period range from 100 to 1000 s. At this period range, a significant fraction of the energy of these modes stays in the mantle where the lateral variation of the structure is relatively small. Thus, the propagation of W phases is not strongly affected by the strong shallow structural heterogeneities caused by the oceans and continents. This is in contrast to the situation with the fundamental mode surface waves which are directly affected by the strong structural heterogeneities near the surface.

Computationally, the mode interpretation is the most straightforward, because W phases can be synthesized by summation of normal modes (Satô & Usami 1962; Saito 1967; Gilbert 1970). For a moment tensor source, we can compute the displacement at a location $\underline{r}$ as a function of time t due to a step function moment tensor source by

$$\underline{u}(\underline{r}, t) =$$

$$\sum_{l,m,n} \left\{ \left[M : {}_n\varepsilon_l^m(\underline{r}_o) \right] {}_n\underline{y}_l^m(\underline{r}) \right\} \frac{1 - \exp(-{}_n\omega_l^m t/2{}_nQ_l^m) \cos {}_n\omega_l^m t}{{}_nc_l^m \, {}_n\omega_l^{m2}}, \quad (1)$$

where ${}_n\underline{y}_l^m(\underline{r})$ is the normal mode (eigenfunction) with the angular order l, azimuthal order m and the radial order n evaluated at the receiver location $\underline{r}$, M is the source moment tensor, ${}_n\varepsilon_l^m\ (\underline{r}_o)$ is the strain tensor computed with the eigenfunction ${}_n\underline{y}_l^m$ at the source location $\underline{r}_o$, ${}_n\omega_l^m$ is the eigen(angular)frequency, ${}_nQ_l^m$ is the quality factor for the corresponding mode and ${}_nC_l^m$ is the energy integral given by

$$ {}_nC_l^m = \int_V \rho\, {}_n\underline{y}_l^m(\underline{r}) \cdot {}_n\underline{y}_l^m(\underline{r}) \mathrm{d}V. \tag{2} $$

Here, ρ is the density, and integration is taken over the Earth's volume V.

The red curve shown in Fig. 1 is the vertical component of W phase computed using (1).

3 RETRIEVAL OF W PHASE

Very broad-band (VBB) records are commonly deconvolved into displacements using the frequency domain method by dividing the frequency spectrum of the VBB records by the instrument response, and inverse-transforming it to the time domain. Our objective is to develop a method for real time operation, and the processing must be done on the time domain in which the data are processed point by point as they become available from the beginning. Since we use a very long period signal, at least to 1000 s, this deconvolution requires special care. We use a method similar to that described by Zhu (2003) for this purpose. In the frequency band of our interest, the response of the VBB system can be written in a form similar to the traditional mechanical seismographs (Wielandt & Streckeisen 1982),

$$ \ddot{y}(t) + 2h\omega_0\dot{y}(t) + \omega_0^2 y(t) = G\dddot{x}(t), \tag{3} $$

where $x(t)$ is the ground-motion displacement, $y(t)$ is the seismograph response, ω_0 is the natural angular frequency of the seismograph, h is the damping constant and G is the gain factor in the unit of counts $(\mathrm{m\ s^{-1}})^{-1}$. For the Streckeisen STS-1 system ω_0 and h are approximately $2\pi/360\ \mathrm{s^{-1}}$ and 0.707, respectively. For the Streckeisen STS-2 system they are approximately $2\pi/120\ \mathrm{s^{-1}}$ and 0.707. For deconvolution, introducing the ground-motion acceleration $a(t) = \ddot{x}(t)$, we rewrite (3) by

$$ \ddot{y}(t) + 2h\omega_0\dot{y}(t) + \omega_0^2 y(t) = G\dot{a}(t). \tag{4} $$

The corresponding difference equation is

$$ \frac{y_{i+2} - 2y_{i+1} + y_i}{\Delta t^2} + 2h\omega_0\frac{y_{i+2} - y_{i+1}}{\Delta t} + \omega_0^2 y_{i+2} = G\frac{a_{i+2} - a_{i+1}}{\Delta t} \tag{5} $$

which can be recast in the form of a recursive filter

$$ a_{i+2} = a_{i+1} + c_2 y_{i+2} + c_1 y_{i+1} + c_0 y_i, \tag{6} $$

where the filter coefficients, c_0, c_1 and c_2 are given by

$$ \begin{aligned} &c_0 = 1/G\Delta t,\ c_1 = -2(1 + h\omega_0\Delta t)/G\Delta t, \text{ and} \\ &c_2 = (1 + 2h\omega_0\Delta t + \Delta t^2\omega_0^2)/G\Delta t. \end{aligned} \tag{7} $$

Applying this filter with the initial condition $a_1 = a_2 = 0$, we obtain the acceleration time series a_i $(i = 1, 2, 3, \ldots, N)$ where N is the total number of data points. Since the main energy of W phase is in the frequency band from 0.0005 to 0.01 Hz, we bandpass filter the acceleration time series in the time domain at this point. The actual passband to be used for our W-phase inversion depends on the magnitude of the events, but in most cases we use a passband from 0.001 to 0.005 Hz (i.e. from 200 to 1000 s). For this filter we use the one-pass Bandpass Butterworth filter written by Dave Harris, which is the same as that used in the SAC, Seismic Analysis Code. Usually, the order of the filter we use is 4.

After filtering, we integrate the acceleration time series twice to obtain the bandpassed displacement records. Zhu (2003) first deconvolved the VBB records into ground-motion velocity $v(t) = \dot{x}(t)$ and integrated it once to displacement. Analytically, this is equivalent to first obtaining acceleration and integrating it twice, as we do in our processing. Because of the very wide frequency band involved, subtle differences exist between the results of these two methods, probably due to round-off errors. For short records, we found no difference, but for long records (e.g. one day), we found the procedure we used (i.e. deconvolution to acceleration, bandpass filtering, followed by twice integration) most satisfactory.

In the above, we used (3) to represent the response of the instrument. However, the response of the broad-band instrument is usually given in poles and zeros instead of constants ω_0, h and G. In principle, it would be possible to compute appropriate recursive filter constants directly from the poles and zeros, but in practice it is cumbersome to construct a recursive filter when many poles and zeros are given. In this paper, we determined the constants ω_0, h and G in such a way that the amplitude response spectrum computed with poles and zeros matches in the least-squares sense with that computed using (4). A similar procedure to estimate ω_0, h and G was used by Kanamori *et al*. (1999) for determining simple recursive filter constants from a given amplitude response over a given frequency band. For most instruments used in the global seismic network, we could find a set of ω_0, h and G which can match the amplitude response spectrum better than 1 per cent over the frequency band relevant to our problem.

For very large earthquakes such as the 2004 Sumatra–Andaman Is. earthquake, the VBB records of global seismic networks are often clipped at the arrival of large amplitude surface waves (see Appendix A). With the traditional frequency-domain deconvolution method, these records are not usable even if a W phase is recorded on scale before the arrival of clipped surface waves. With the use of time-domain method, we can use these records for inversion. An example is shown in Fig. 3.

Since the group velocity of W phase ranges from 4.5 to 9.0 km $\mathrm{s^{-1}}$, most of the W-phase energy arrives within a short time interval after the P arrival. We computed W phases as a function of distance and found that a time window with a duration of 15Δ s (Δ in degree) after the P arrival can contain the most of W-phase energy. In this paper, we use this time window to extract W phases but the window could be widened considerably at short distances, if so desired.

After having extracted W phases from all the stations, we concatenated them in the order of increasing epicentral distance. The concatenation in the order of increasing distance is not essential for inversion, but is useful for inspecting the data and the quality of the fit. The result is a concatenated W phase as shown in Fig. 4. This is the time series to be used as data in inversion.

4 INVERSION

In inversion of W phases (hereafter, abbreviated to WP inversion), we assume a spatial point source as is done in the Harvard and Global Centroid Moment Tensor (hereafter, abbreviated to CMT) inversion (Dziewonski *et al.* 1981; Ekström et al. 2005). Their catalogues are in the web site for Harvard CMT catalogue and global CMT catalogue, respectively. The point source location is called the centroid location. The point source varies in time with a given

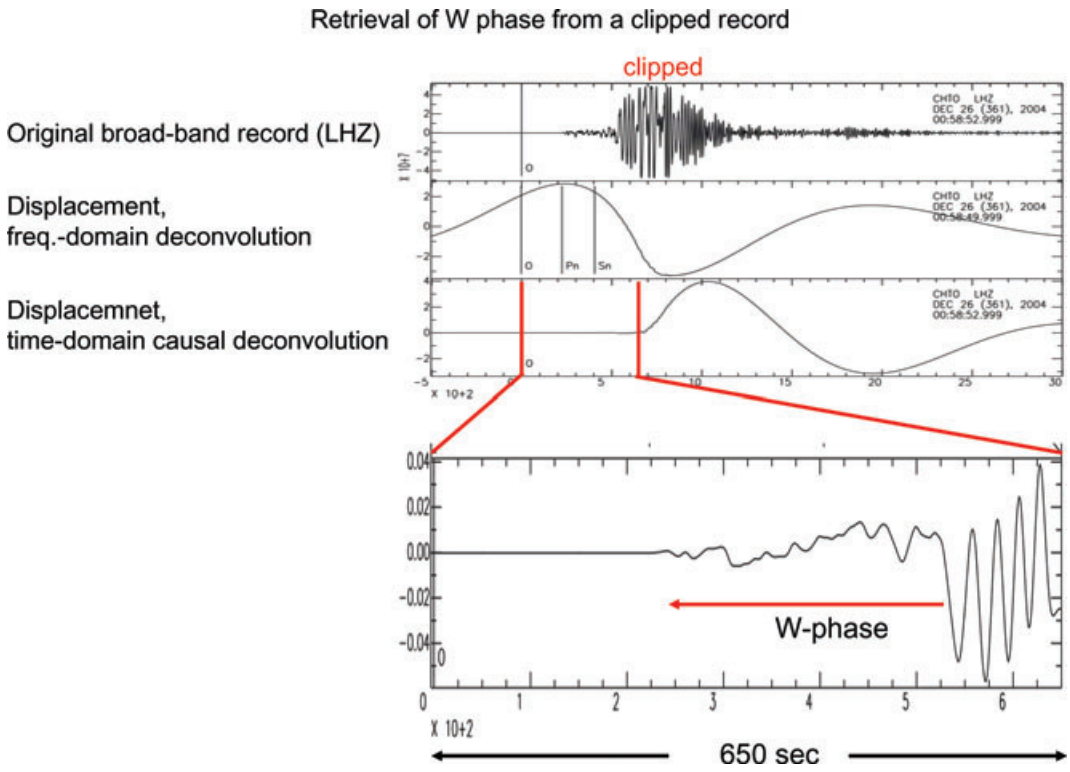

Figure 3. Example of frequency-domain deconvolution (second trace) and recursive time-domain deconvolution (third and fourth traces) of a clipped very broad-band record (top trace). With the frequency-domain deconvolution, the wrap-around effect from the clipped portion made the W phase portion of the record unusable. With the time-domain deconvolution, the time series is processed point by point, and the W phase can be recovered up to the time when clipping occurred.

time history. If the centroid location and the source time history are known, the inversion is linear with respect to the moment tensor elements M_{ij}, and can be formulated as

$$\begin{pmatrix} u_{w1}^{1,1} & u_{w1}^{2,2} & * & * & * & u_{w1}^{2,3} \\ u_{w2}^{1,1} & u_{w2}^{2,2} & * & * & * & u_{w2}^{2,3} \\ u_{w3}^{1,1} & u_{w3}^{2,2} & * & * & * & u_{w3}^{2,3} \\ * & * & * & * & * & * \\ * & * & * & * & * & * \\ * & * & * & * & * & * \\ * & * & * & * & * & * \\ * & * & * & * & * & * \\ * & * & * & * & * & * \\ * & * & * & * & * & * \\ * & * & * & * & * & * \\ u_{wN}^{1,1} & u_{wN}^{2,2} & * & * & * & u_{wN}^{2,3} \end{pmatrix} \begin{pmatrix} M_{11} \\ M_{22} \\ M_{33} \\ M_{12} \\ M_{13} \\ M_{23} \end{pmatrix} = \begin{pmatrix} u_{w1} \\ u_{w2} \\ u_{w3} \\ * \\ * \\ * \\ * \\ * \\ * \\ * \\ * \\ u_{wN} \end{pmatrix}, \tag{8}$$

where M_{kl} are the k-l element of the source moment tensor, $u_{wi}^{k,l}(t)$ is the displacement at station i computed for a moment tensor with only $M_{kl} = 1$ (i.e. $M_{ij} = \delta_{il} > \delta_{jk}$), and $u_{wi}(t)$ is the observed W phase at station i. This equation holds for any component of displacement, but we use only the vertical component in this paper, and all the displacements here are understood as the vertical component. To compute $u_{wi}^{k,l}(t)$, we first compute the step function response for a unit moment tensor element. We call the step function response the Green's function. Then convolving the Green's function with the source time function (i.e. the moment rate function), and filtering it with the same bandpass filter applied to the observed seismograms, we obtain $u_{wi}^{k,l}(t)$. We call $u_{wi}^{k,l}(t)$ the synthetic displacements for a unit source. We will discuss how we compute the Green's functions in the next section.

The column vector on the right-hand side is the concatenated observed W phase, and the column vectors of the matrix on the left-hand side are the concatenated synthetic displacements for a unit source computed with each one of the six basic moment tensor elements.

Inversion can be done with the use of the least-squares method for all the six elements of the moment tensor, or with some linear constraints, for a fewer number of elements. For example if we assume that the source involves no net volume change, we can use $M_{33} = -(M_{11} + M_{22})$ and solve (8) for the remaining five elements. In this case the inversion remains linear.

As mentioned above, it is assumed that the centroid location and the source time function are known. We follow the practice used by the Harvard Centroid Moment Tensor solution, and use a triangular source function defined by two parameters, half duration, t_h, and the centroid delay, t_d, to represent the moment rate function. The half duration is the half width of the triangular moment rate function, and the centroid delay is the temporal position of the centre of the triangle measured from the assumed origin time. In the real-time situation, only the hypocentral location (i.e. the location of the initial rupture rather than the centroid location) and the origin time determined from the P-wave arrivals are known. Thus, we need to estimate t_h, t_d and the centroid location. However, since W phase is a

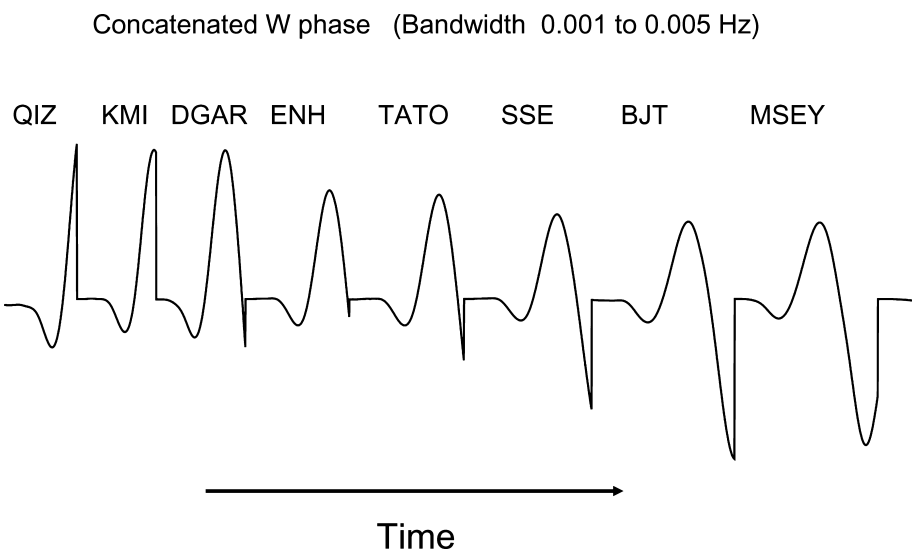

Figure 4. Concatenated W phase.

very long-period wave with a fast group velocity similar to *P* wave, these parameters need to be known only approximately. Depending on the required quality of the solution, we can proceed as follows. Since the records are filtered at very long period, the half duration is relatively unimportant. The hypocentre location can be used as the first approximation of the centroid location. Because of the fast group velocity of W phase, the solution is generally adequate for rapid tsunami warning purposes even with this approximation. The most critical parameter is the delay (time-shift), t_d. Because it shifts the W phase in time in the same direction at all the stations by the same amount, inappropriate choice of t_d results in large misfits of the waveforms. To the first order, t_d can be roughly estimated from the preliminary magnitude. The preliminary magnitude can be estimated from the amplitude of W phase by the method to be described later. However, for anomalous events such as slow tsunami earthquakes, t_d can be significantly longer than that estimated from the preliminary magnitude. The best estimate of t_d can be obtained by a simple 1-D grid search by minimizing the root mean square (rms) of the waveform misfit.

Having determined the optimal t_d, inversion can be made with the hypocentral location as the centroid location. This inversion usually yields a solution good enough for fast tsunami warning purposes, but with another grid search, we can estimate the optimal centroid location. We usually fix the depth at the hypocentral depth. The inversion with these two grid searches yields our WP inversion solution. For purposes of comparison with the Harvard and Global CMT solutions, we also perform WP inversion using the same t_d, t_h and the centroid location as those given by the Harvard and Global CMT.

With this parametrization, the least-squares inversion can be done without any smoothing constraint.

5 GREEN'S FUNCTIONS

For WP inversion, we need to compute only the vertical component Green's functions, but, for the sake of generality, we discuss how we compute all the components in the following.

In general, we need to compute three components of displacement for six moment tensor elements. Thus, at first sight, we need to compute a total of 18 Green's functions for each station. However, for the case of a spherically symmetric Earth these are not linearly independent. The number of linearly independent Green's functions is reduced significantly because of the symmetry of the problem.

For a given depth and distance, consider a station at point P located due north of the source (i.e. azimuth, $\Phi = 0$). Then, only 10 out of 18 are non-zero as shown below. We use the same coordinate system as that used in the Harvard Centroid Moment Tensor project, that is, (r, θ, ϕ) for [vertical (up), south, east]. Then, from the symmetry of the problem,

(1) For a vertical dipole (i.e. $M_{rr} = 1$), $u_\phi = 0$.
(2) For a north-south dipole (i.e. $M_{\theta\theta} = 1$), $u_\phi = 0$.
(3) For an east-west dipole (i.e. $M_{\phi\phi} = 1$), $u_\phi = 0$.
(4) For a shear source $M_{r\theta} = 1$, $u_\phi = 0$.
(5) For a shear source $M_{r\phi} = 1$, $u_r = 0$ and $u_\theta = 0$.
(6) For a shear source $M_{\theta\phi} = 1$, $u_r = 0$ and $u_\theta = 0$.

Thus, if we denote the k component of displacement due to a source $M_{lm} = 1$ by $u_k(t; l, m)$, we can write the three components of the displacement at point P by

$$\begin{aligned} u_r(t) &= M_{rr}u_r(t;r,r) + M_{\theta\theta}u_r(t;\theta,\theta) + M_{\phi\phi}u_r(t;\phi,\phi) \\ &\quad + M_{r\theta}u_r(t;r,\theta) \\ u_\theta(t) &= M_{rr}u_\theta(t;r,r) + M_{\theta\theta}u_\theta(t;\theta,\theta) + M_{\phi\phi}u_\theta(t;\phi,\phi) \\ &\quad + M_{r\theta}u_\theta(t;r,\theta) \\ u_\phi(t) &= M_{r\phi}u_\phi(t;r,\phi) + M_{\theta\phi}u_\phi(t;\theta,\phi). \end{aligned} \tag{9}$$

To compute the displacement at point Q with azimuth Φ, we rotate the moment tensor around the vertical axis at the source by Φ and perform the same analysis as above. The rotated moment tensor M' is given by

$$M' = RMR^T,$$

where

$$R = \begin{pmatrix} \cos\Phi & \sin\Phi & 0 \\ -\sin\Phi & \cos\Phi & 0 \\ 0 & 0 & 1 \end{pmatrix}.$$

Table 1. Centroid parameters used for WP inversion, the nodal planes and M_w determined by inversion.

Event	Inversion	θ_s (°)	λ_s (°)	d_s (km)	t_d (s)	t_h (s)
2003 Tokachi-oki	1. PDE + optimized t_d	41.81	143.91	27	30	30
	2. Optimized t_d and centroid	42.15	143.85	27	30	30
	3. With CMT centroid	42.21	143.84	28.24	31.81	33.5
2007 Sumatra	1. PDE + optimized t_d	−4.52	101.38	30.0	53	53
	2. Optimized t_d and centroid	−3.75	101.0	30.0	53	53
	3. With CMT centroid	−3.7	101.0	23.33	51.17	39.0
2004 Sumatra	1. PDE + optimized t_d	3.30	95.78	20.0	150	150
	2. With CMT centroid	3.09	94.26	28.61	138.95	95
2006 Java	1. PDE + optimized t_d	−9.25	107.41	34.0	70	70
	2. With CMT centroid	−10.2	107.78	20.	69.6	13.9
2007 Kuril Is.	1. With CMT centroid	46.17	154.80	12.0	26.9	27.4

Event	Inversion	Nodal plane-1 (strike/dip/rake)	Nodal plane-2 (strike/dip/rake)	M_w
2003 Tokachi-oki	1. PDE + optimized t_d	19.1/81.1/79.0	−109.4/14.1/140.7	8.24
	2.Optimized t_d and centroid	29.0/82.6/84.3	−113.1/9.3/127.5	8.31
	3. With CMT centroid	30.5/81.3/84.0	−114.7/10.5/124.3	8.27
2007 Sumatra	1. PDE + optimized t_d	151.4/78.9/97.0	−61.0/13.0/58.2	8.41
	2.Optimized t_d and centroid	125.3/82.4/86.2	−28.3/8.5/116.2	8.50
	3. With CMT centroid	125.7/80.4/85.6	−29.4/10.6/114.5	8.44
2004 Sumatra	1. PDE + optimized t_d	149.1/86.4/92.5	−65.6/4.4/55.4	9.33
	2. With CMT centroid	133.8/81.1/90.1	−46.7/8.9/89.5	9.01
2006 Java	1. PDE + optimized t_d	93.5/85.2/87.6	−60.2/5.4/116.1	7.83
	2. With CMT centroid	99.5/79.3/86.3	−61.5/11.3/108.6	7.62
2007 Kuril Is.	1. With CMT centroid	228.0/71.6/−103.3	84.8/22.5/-55.4	8.14

Then, the three components of the displacement at point Q can be written as

$$\begin{aligned} u_r(t) &= M'_{rr}u_r(t;r,r) + M'_{\theta\theta}u_r(t;\theta,\theta) + M'_{\phi\phi}u_r(t;\phi,\phi) \\ &\quad + M'_{r\theta}u_r(t;r,\theta) \\ u_\theta(t) &= M'_{rr}u_\theta(t;r,r) + M'_{\theta\theta}u_\theta(t;\theta,\theta) + M'_{\phi\phi}u_\theta(t;\phi,\phi) \\ &\quad + M'_{r\theta}u_\theta(t;r,\theta) \\ u_\phi(t) &= M'_{r\phi}u_\phi(t;r,\phi) + M'_{\theta\phi}u_\phi(t;\theta,\phi), \end{aligned} \tag{10}$$

where

$$\begin{aligned} M'_{\phi\phi} &= M_{\phi\phi}\cos^2\Phi - 2M_{\phi\theta}\sin\Phi\cos\Phi + M_{\theta\theta}\sin^2\Phi \\ M'_{\theta\theta} &= M_{\phi\phi}\sin^2\Phi + 2M_{\phi\theta}\sin\Phi\cos\Phi + M_{\theta\theta}\cos^2\Phi \\ M'_{rr} &= M_{rr} \\ M'_{\phi\theta} &= -\frac{1}{2}\left(M_{\theta\theta} - M_{\phi\phi}\right)\sin 2\Phi + M_{\phi\theta}\cos 2\Phi \\ M'_{\phi r} &= M_{\phi r}\cos\Phi - M_{\theta r}\sin\Phi \\ M'_{\theta r} &= M_{\theta r}\cos\Phi + M_{\phi r}\sin\Phi. \end{aligned} \tag{11}$$

Note that the expressions given above have been derived with the symmetry arguments and are completely general; no distinction is made between spheroidal and toroidal modes. However, actual computations of $u_k(t;l,m)$ must be made using the explicit expressions involving eigenfunctions and eigen values (e.g. Kanamori & Given 1981).

Here we pre-computed the Green's functions for three component displacements for a distance range of $0^\circ \le \Delta \le 90^\circ$ with an interval of 0.1° and for a depth range of 0–760 km. The depth intervals vary from 2 to 10 km as the depth increases. Although we need only long-period modes for the first several overtones for the present study, we computed, for completeness sake, all the modes to shorter periods. Our Green's function data base has 103 000 spheroidal modes 63 000 toroidal modes, and 152 radial modes and is complete to a period of 12 s.

6 EXAMPLES

Here we show several examples of WP inversion. Table 1 summarizes the hypocentral, centroid and source time function parameters for the events discussed here.

In these examples we assume that $M_{rr} + M_{\theta\theta} + M_{\phi\phi} = 0$ (i.e. no net volume change).

6.1 2003 Tokachi-oki earthquake ($M_w = 8.3$)

The data used are the 1 sps (sample-per-second) (i.e. LH channel) vertical component records taken from the data base at the Incorporatel Research Institutions for Seismology (IRIS) over a duration of 15Δ(degree) s after the *P* arrival. We bandpass filter them from 0.001 to 0.005 Hz and concatenate them in the order of distance. Then, we compute the synthetics for a unit source for each station using the Green's functions by convolving them with a triangular source time function having a half duration, t_h, bandpass filtering them with the same filter as that applied to the data, and delaying them by t_d. We determined t_d by a simple grid search (one-dimensional) by minimizing the rms of the waveform misfit. Fig. 5(a) shows the result of inversion with $t_d = t_h = 30$ s. The choice of t_h is not critical; it can be either held at the initial value estimated from the preliminary magnitude, or is set equal to t_d. The steep nodal line of this solution is rotated by about 12° with respect to the CMT solution, but M_w is nearly the same. This solution would be good enough for fast tsunami warning purposes. With another spatial grid search in which an optimal centroid location is determined by minimizing the rms misfit, we can obtain a solution very similar to the CMT solution, as shown in Fig. 5(b). Fig. 5(c) shows the result of WP inversion with the CMT centroid parameters. Fig. 6 compares the concatenated observed W phase with that computed for the solution given in Fig. 5(c). The overall agreement between the observed and synthetics is generally good.

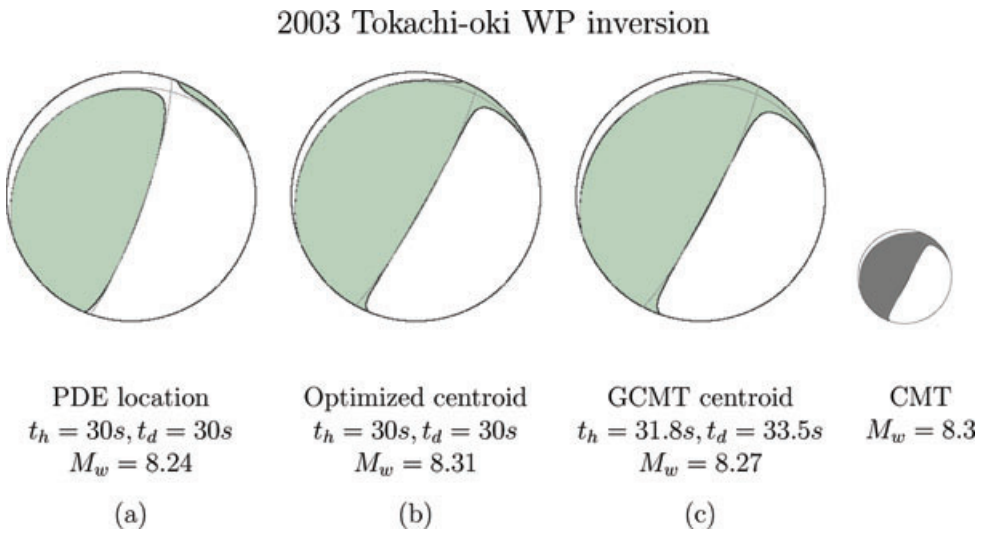

Figure 5. WP inversion results for the 2003 Tokachi-oki earthquake.

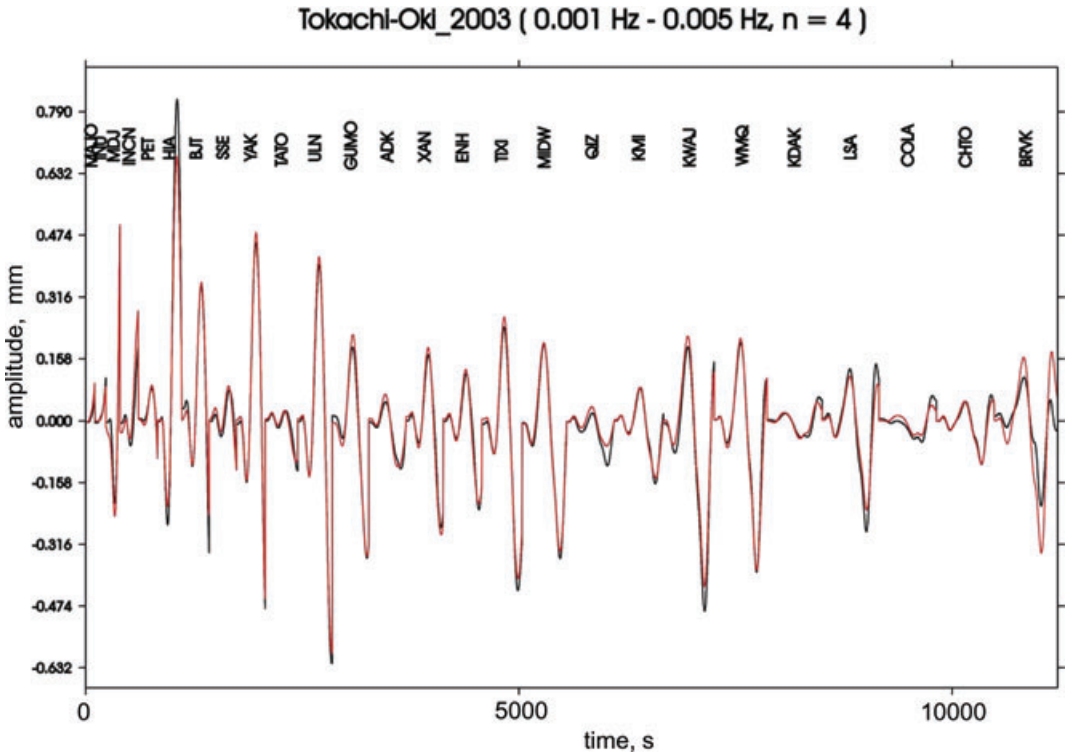

Figure 6. Concatenated observed (black trace) and synthetic (red trace) W phase. The window length (in s) is Δ(in degree)/n min. In this case $n = 4$.

Optimization of the time delay t_d can be done easily in the real-time situation, because the synthetics need not be recomputed. To determine the optimal centroid location, all the synthetics need to be recomputed which requires additional time, but since all the Green's functions have been pre-computed, this process is not prohibitively time consuming. Depending on the required accuracy of the solution, one can use the solution with an optimized t_d and the PDE location, or with an optimized t_d together with an optimized centroid location. The latter solution is usually close to the WP inversion solution with the CMT centroid parameters. We cannot use the CMT centroid parameters in the real-time situation, but the WP inversion solution with the CMT centroid source parameters are useful for comparison of WP inversion and CMT inversion.

6.2 2007 Sumatra earthquake ($M_w = 8.4$)

We made a similar analysis for the 2007 Sumatra earthquake, and the results are shown in Figs 7 and 8. The PDE location is at (-4.52°, 101.38°, depth = 30 km) and the CMT centroid location is at (-3.7°, 101.0°, depth = 23.33 km). For the inversion with the PDE location, the delay time t_d determined with a grid search

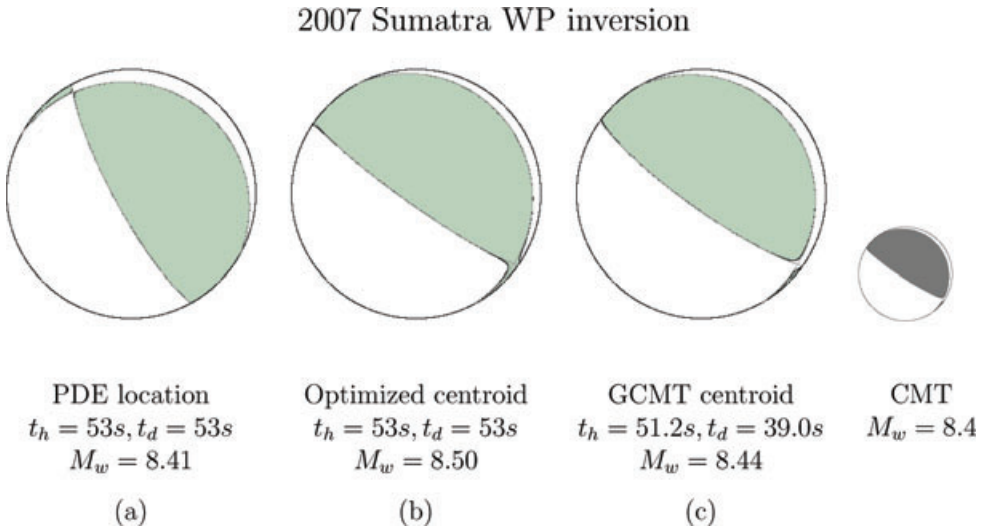

Figure 7. WP inversion results for the 2007 Sumatra earthquake.

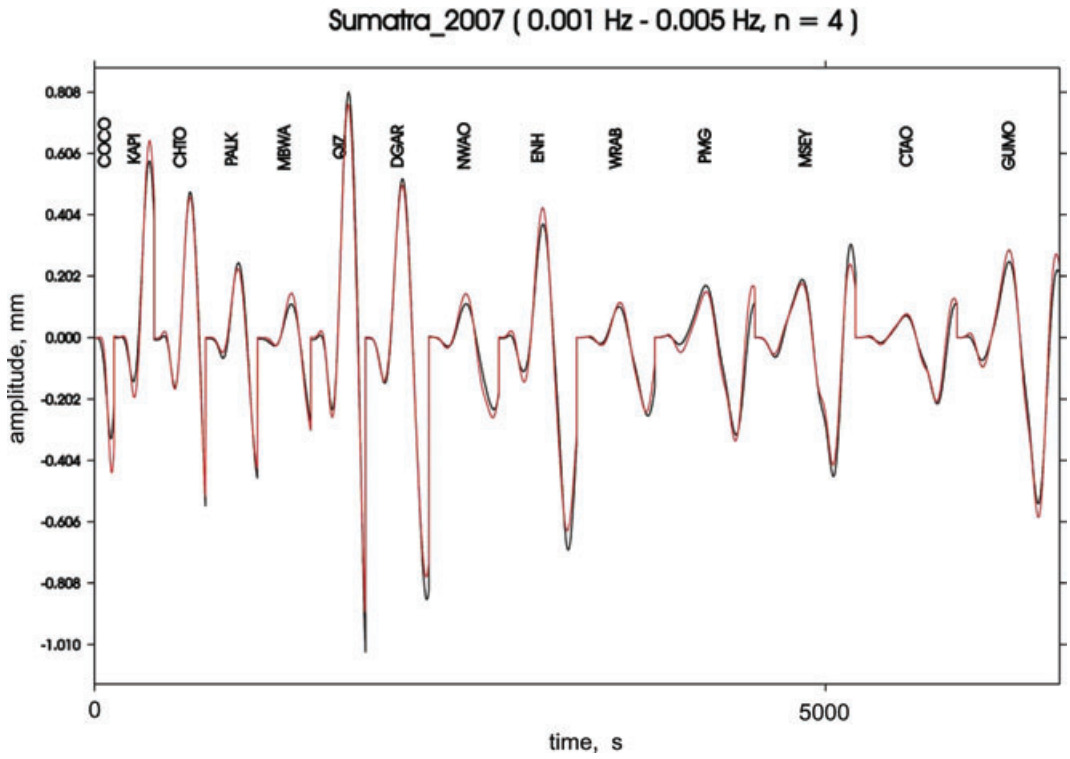

Figure 8. Concatenated observed (black trace) and synthetic (red trace) W phase. The window length (in s) is Δ(in degree)/n min. In this case $n = 4$.

is 53 s. We assume $t_h = t_d$ for this inversion. Despite the fairly large difference between the PDE location and the centroid location (about 100 km), the inversion with the PDE location (Fig. 7a) yields a solution good enough for tsunami warning purposes. The steep nodal plane is rotated by about 26° from the CMT solution, but M_w is about the same. Another grid search yields an optimal centroid location at (−3.75°, 101.0°, 30 km), and the solution (Fig. 7b) is essentially the same as that with the CMT centroid parameters (Fig. 7c). The match between the observed and synthetic W phases is good as shown in Fig. 8.

6.3 2004 Sumatra–Andaman earthquake ($M_w = 9.2$)

The PDE location is at (3.30°, 95.78°, depth = 10 km) and the CMT centroid location is at (3.09°, 94.26°, depth = 23.33 km). For the inversion with the PDE location the delay time t_d determined with a grid search is 150 s. The solution with the PDE location with $t_d = t_h = 150$ s and that with the CMT centroid parameters are shown in Figs 9(a) and (b). The difference in M_w between the two solutions is due to the difference in dip angle. Since the dip angle is not well constrained, the difference in M_w is not significant.

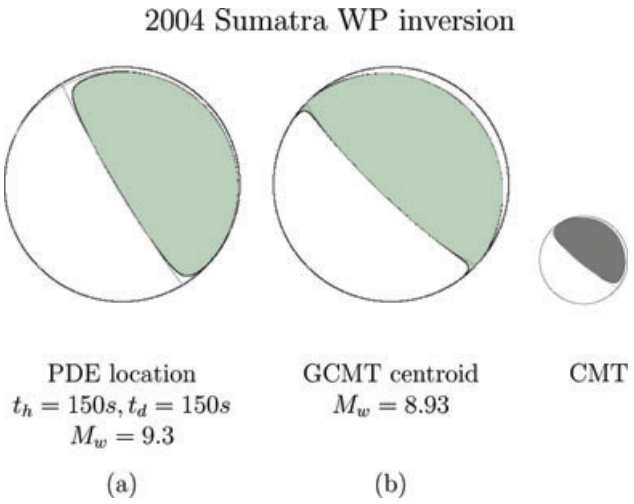

Figure 9. WP inversion results for the 2004 Sumatra earthquake.

Fig. 10 compares the observed W phases with the synthetics computed for the solution with the CMT centroid parameters. The waveform match is generally good except at a few stations. For example, the observed amplitude at NWAO which is in the azimuth away from the rupture propagation is considerably smaller than the predicted by the model. This disagreement is due to directivity. However, the disagreement is not as prominent as those seen in the commonly used body- and surface wave inversions (e.g. Ammon *et al*. 2005). Since W phase has very long wavelength and fast group velocity, the waveforms are much less sensitive to the source directivity. Thus, WP inversion is suitable for inversion of the source represented as a point source. As mentioned earlier, propagation of W phase is not strongly affected by the shallow structural heterogeneities caused by oceans and continents, which enables us to achieve the excellent fit of the waveforms. Fig. 11 shows the comparison of the observed and synthetic waveforms for all the stations. The portions bracketed by the two red dots are the W phase used for inversion, and the later arriving large amplitude surface waves are not used for inversion. Note that wherever the surface waves are on scale, the waveform match is generally good even if this portion is not used for inversion. At many stations, especially those at shorter distances, the surface wave portion displays obviously anomalous behaviour due to either clipping or being driven beyond the linear range. Even at these stations, W phase is on scale and usable. This is another obvious merit of using WP inversion.

6.4 2006 Java tsunami earthquake ($M_w = 7.7$)

The PDE location is at (−9.25°, 107.41°, depth = 34 km) and the CMT centroid location is at (−10.2°, 107.78°, depth = 20.0 km). For the inversion with the PDE location, the delay time t_d determined with a grid search is 70 s. The solution with the PDE location with $t_d = t_h = 70$ s and that with the CMT centroid parameters are shown in Fig. 12. Fig. 13 compares the observed W phases with the synthetics computed for the solution with the CMT centroid parameters.

Although the steep nodal plane of the solution with the PDE location is rotated by 6° with respect to that with the CMT centroid parameters, the overall mechanism and M_w are similar, and the solution with the PDE location should be good enough for tsunami warning purposes.

In general, if the delay time t_d is estimated with a simple grid search, the inversion with the PDE location yields a solution good enough for tsunami warning purposes. If an optimal centroid can be determined with a spatial grid search, the solution of WP inversion

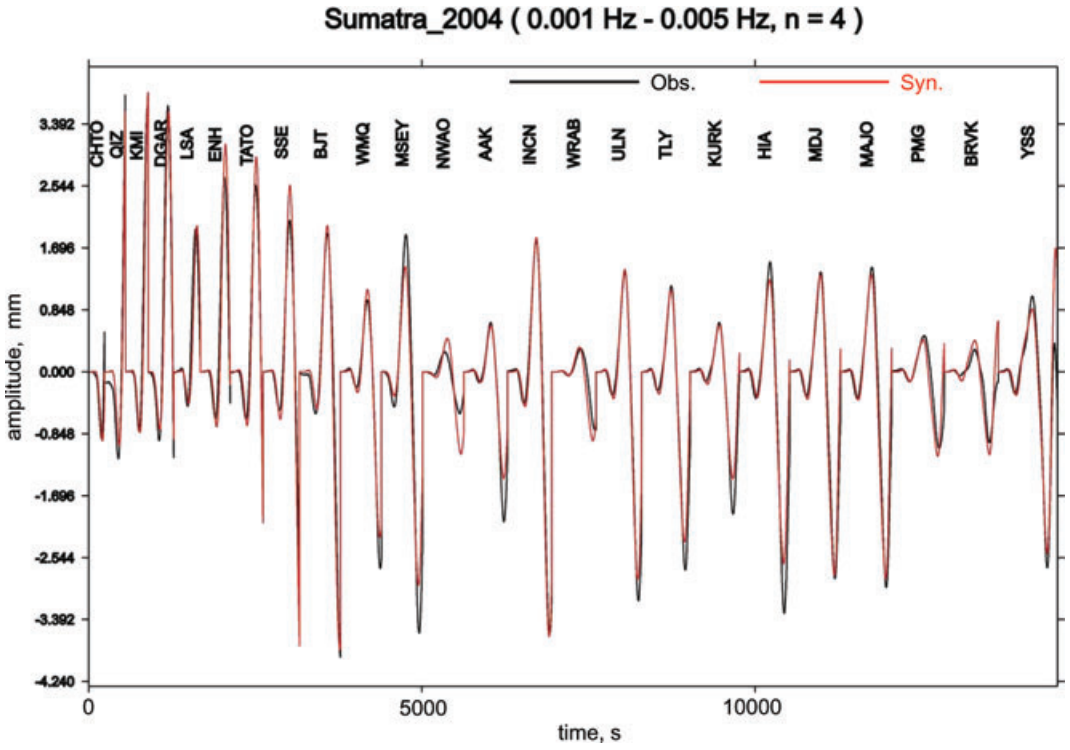

Figure 10. Concatenated observed (black trace) and synthetic (red trace) W phase. The window length (in s) is Δ(in degree)/n min. In this case $n = 4$.

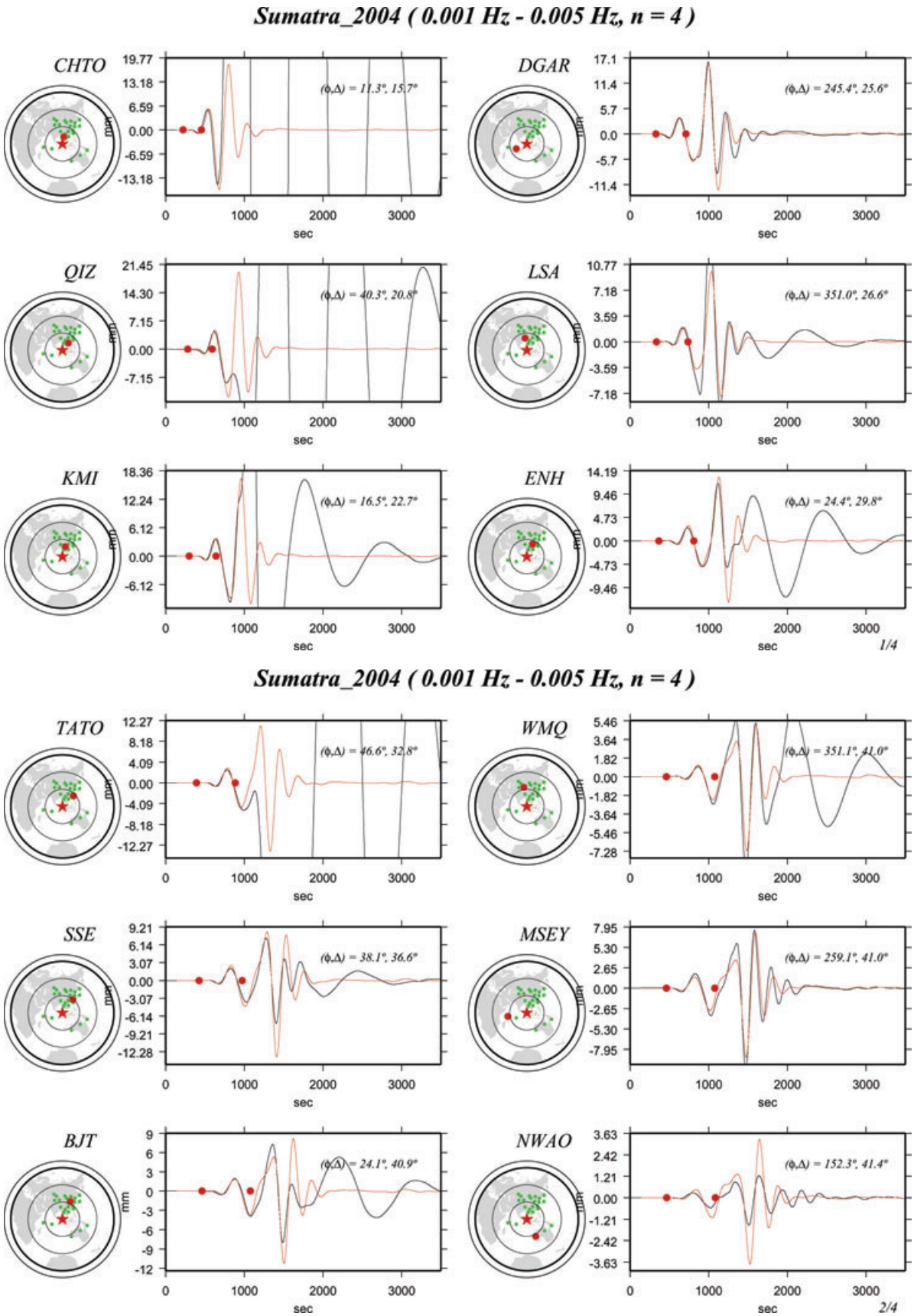

Figure 11. Comparison of the observed (black trace) and synthetic (red trace) waveforms. Two red dots on the trace indicate the end points of the W phase inverted.

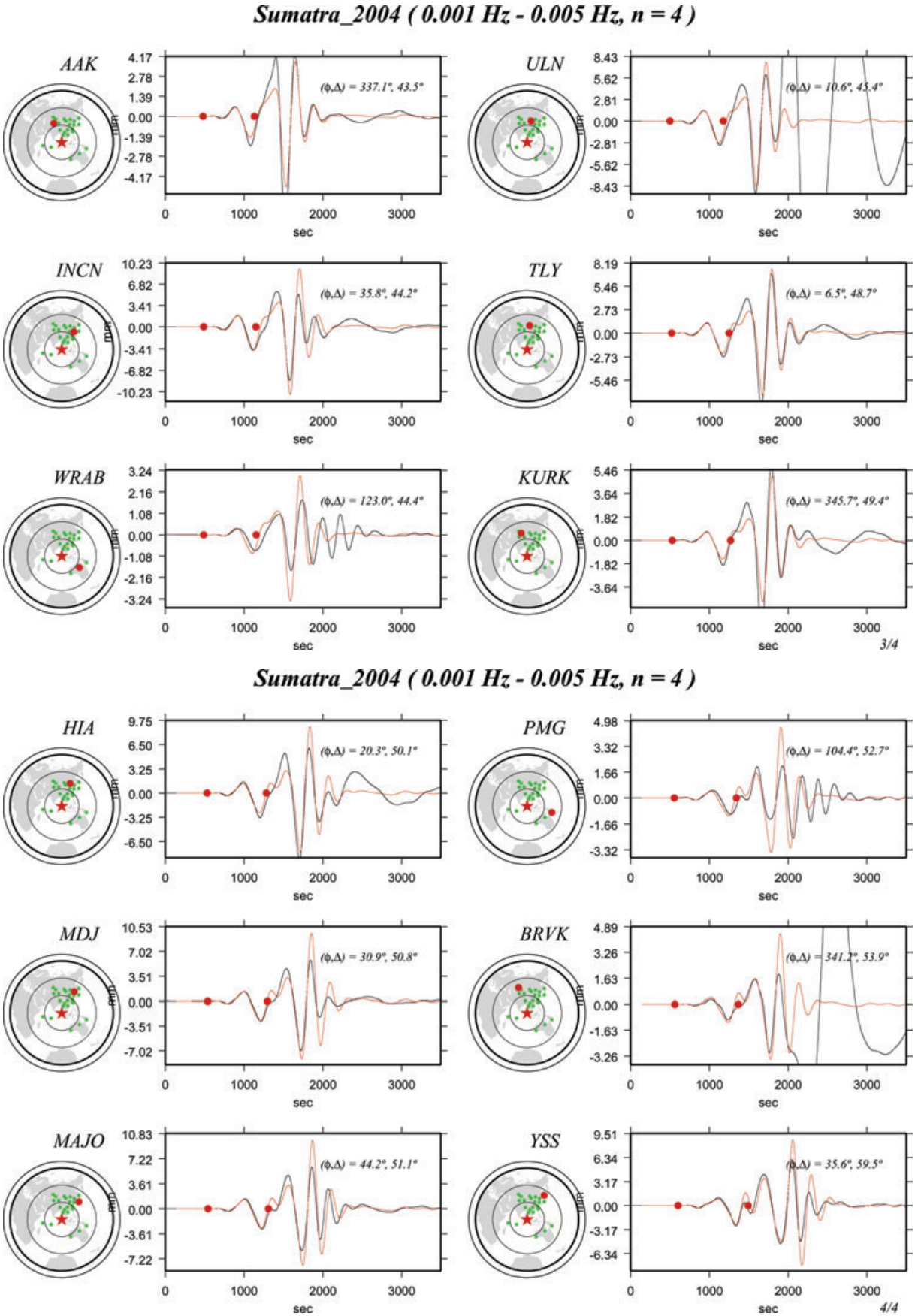

Figure 11. (*Continued*).

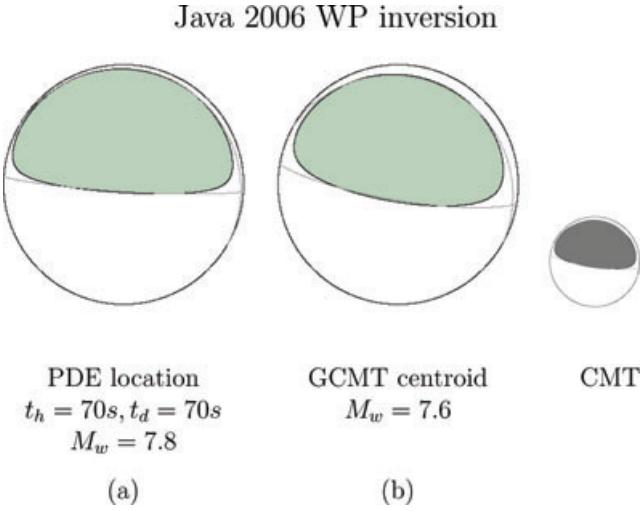

Figure 12. WP inversion results for the 2006 Java slow earthquake

is usually very similar to the Harvard and Global CMT solution. However, for a very large event like the 2004 Sumatra–Andaman earthquake, exactly what the CMT centroid location determined by minimizing the rms of misfit means is unclear, and more detailed analyses would be necessary to determine the most meaningful CMT parameters. Thus, for rapid tsunami warning purposes, the solution with the PDE location is considered adequate.

Since WP inversion covers a very long period range of the source spectrum, apart from tsunami warning purposes, it is interesting to compare WP inversion with the CMT centroid parameters with the standard CMT inversion. If the source is relatively simple, the two inversions are expected to yield a similar mechanism. However, if the results of the two inversions differ, it suggests that the source has some additional feature beyond the CMT mechanism. Our preliminary analyses show that for most earthquakes if the same centroid parameters are used the solutions determined by WP inversion and CMT inversion are almost identical. One exception is the 2007 Kuril Is. earthquake ($M_w = 8.1$, Fig. 14). For this event, the strike of the north dipping nodal plane of the CMT solution is almost E–W. In contrast, it is 48° NE (i.e., 228°) for the WP inversion mechanism. This strike is more or less parallel to the strike of the aftershock area and the trench. Since the difference in the solution between WP and CMT is large, we include the fault parameters determined by the WP inversion in Table 1. At present, we have not investigated the cause of this difference. A more systematic comparison for all the events with $M_w \geq 7$ is in progress.

7 TRADEOFF BETWEEN SPEED AND DISTANCE RANGE

As the end of the time window is given by P arrival time + 15 Δ, the key factor which determines the speed of WP inversion is the distance range to be used for inversion. The larger the distance range used, more stations can be used, and the reliability would increase. However, we need to wait longer. Thus, we have a direct trade off between speed and reliability. In our experience, with the present density of the global network, if we use the stations up to $\Delta = 50°$, we can usually obtain good solutions. Then as shown in Fig. 15, we can collect all the data at about 20 min after the origin time of the earthquake. If we reduce the distance range, the time can be shortened. As Fig. 16 illustrates, the solution does not change significantly even if we reduce the distance range to 30° as long as the azimuthal coverage remains the same. In this case, the time required to collect all the data can be reduced to 15 min after the origin time.

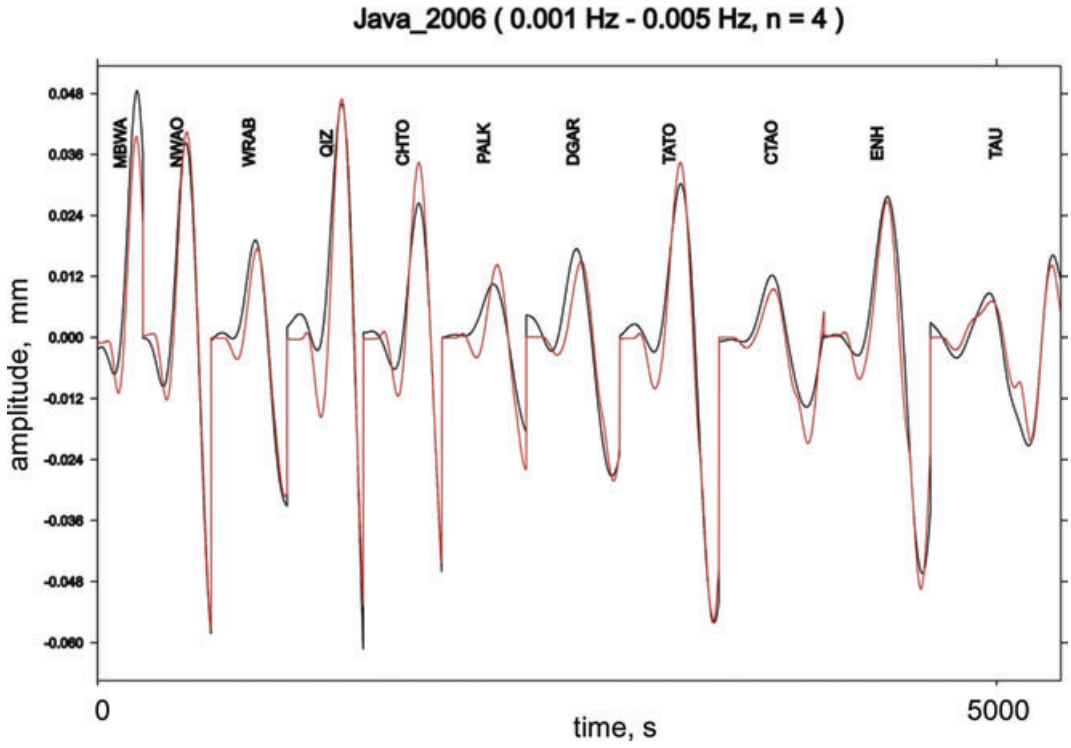

Figure 13. Concatenated observed (black trace) and synthetic (red trace) W phase. The window length (in s) is Δ(in degree)/n min. In this case $n = 4$.

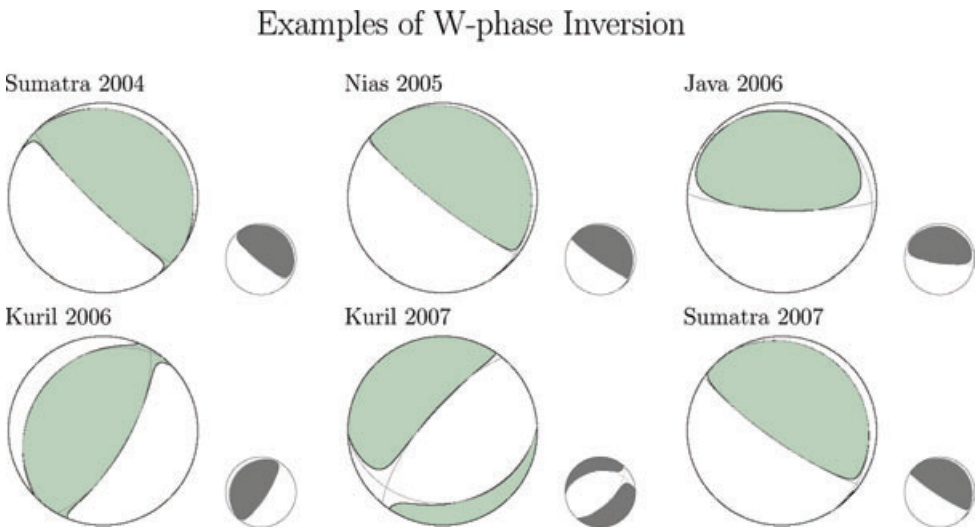

Figure 14. Comparison of WP inversion solution (large) and CMT solution (small).

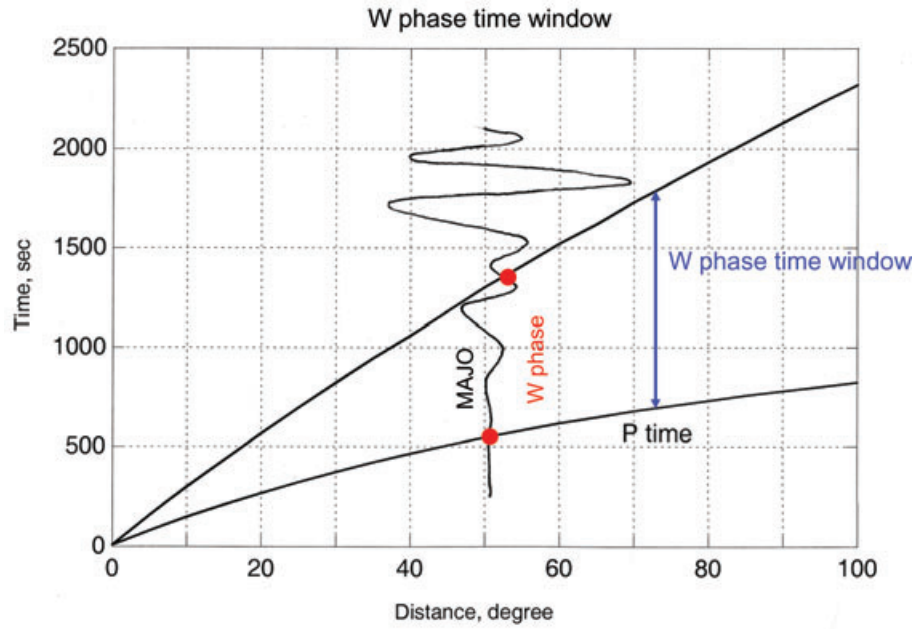

Figure 15. Illustration of the W-phase time window. At $\Delta = 50^\circ$ and 30°, the end of time window is at about 21 and 13 min, respectively.

Since the method is linear and all the Green's functions have been pre-computed, the computation time is very short. Depending on the required quality of the solution, some iterations need to be made for grid search, which requires extra computer time. The deconvolution of the data is done continuously without waiting for the end of the time window. How much overhead will be required would depend on the required accuracy and reliability and on the details of data processing, but Fig. 15 basically governs the required time.

8 IMPLEMENTATION ISSUES

For practical tsunami warning purposes, speed and robustness of the method are critical. Here we discuss how best W phase tsunami warning method can be implemented for practical purposes.

The time-domain deconvolution method we developed allows us to constantly monitor W phases on a display. At this point it would be desirable to remove the stations which are either malfunctioning or noisy at long period. This would greatly simply the screening process during inversion at a later stage. When a large earthquake occurred, an operator can immediately see the W phases from all the stations, recognize the occurrence of the event and even measure the amplitude to get an approximate estimate of the magnitude. Fig. 17 is an example of such a display. It is assumed that the hypocentral location has been provided so that the traces can be approximately lined up with respect to the *P* time. With this display the occurrence of an event would be obvious to an on-duty operator, which will minimize the possibility of false alarms and missed alarms.

The amplitude of W phase is a function of the seismic moment, the distance, and the azimuth of the station. In general, if the

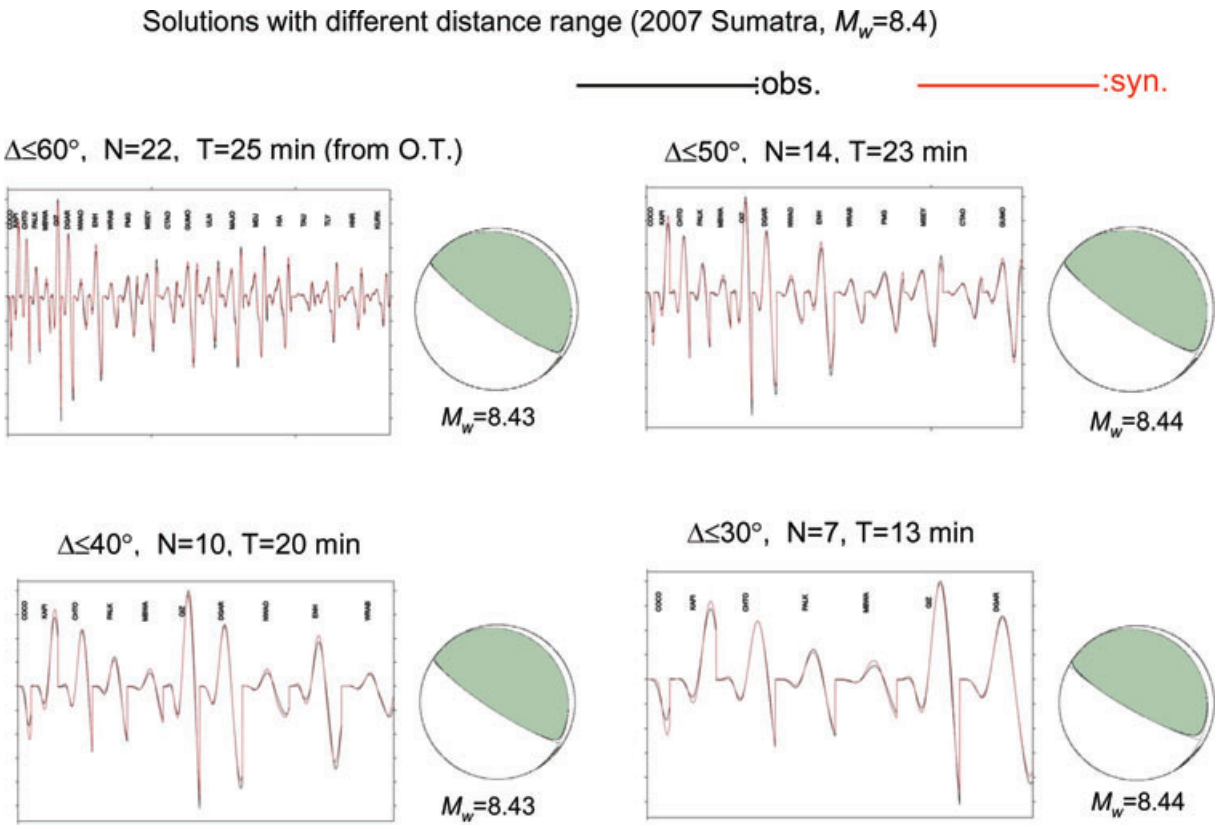

Figure 16. Inversion results for the 2007 Sumatra earthquake with different distance cut off. For this event, the inversion yields a good result even with the data up to only 30°.

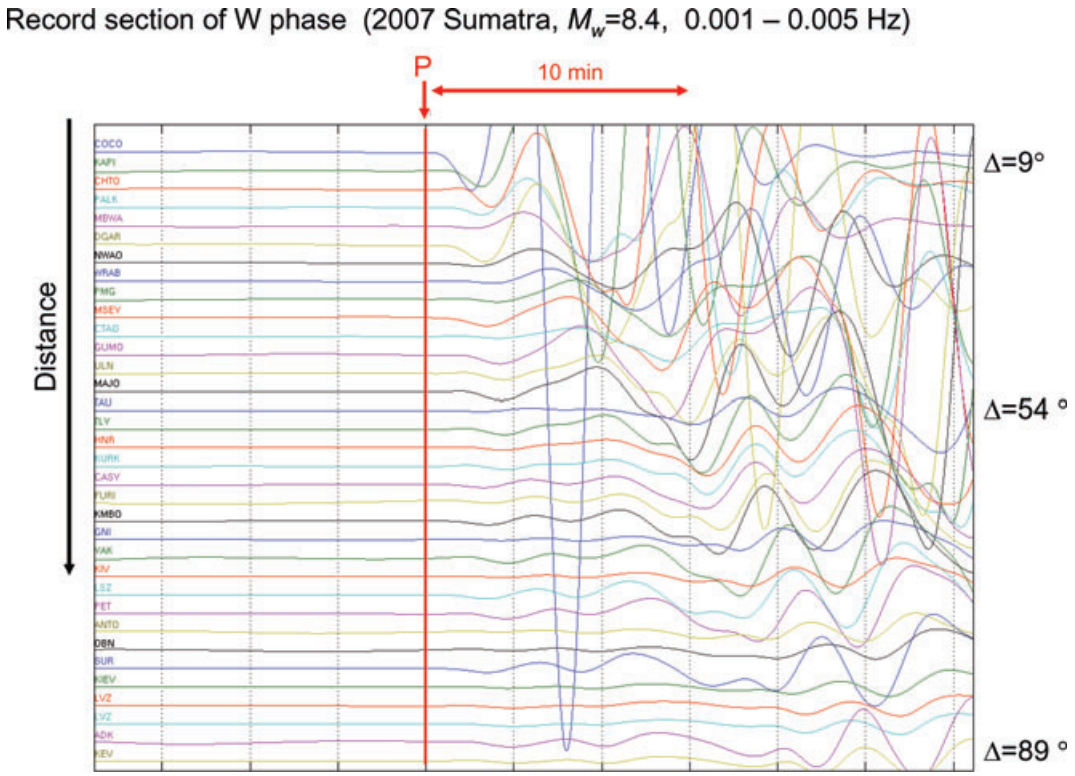

Figure 17. W phase record section for the 2007 Sumatra earthquake. The records are lined up at the *P* time.

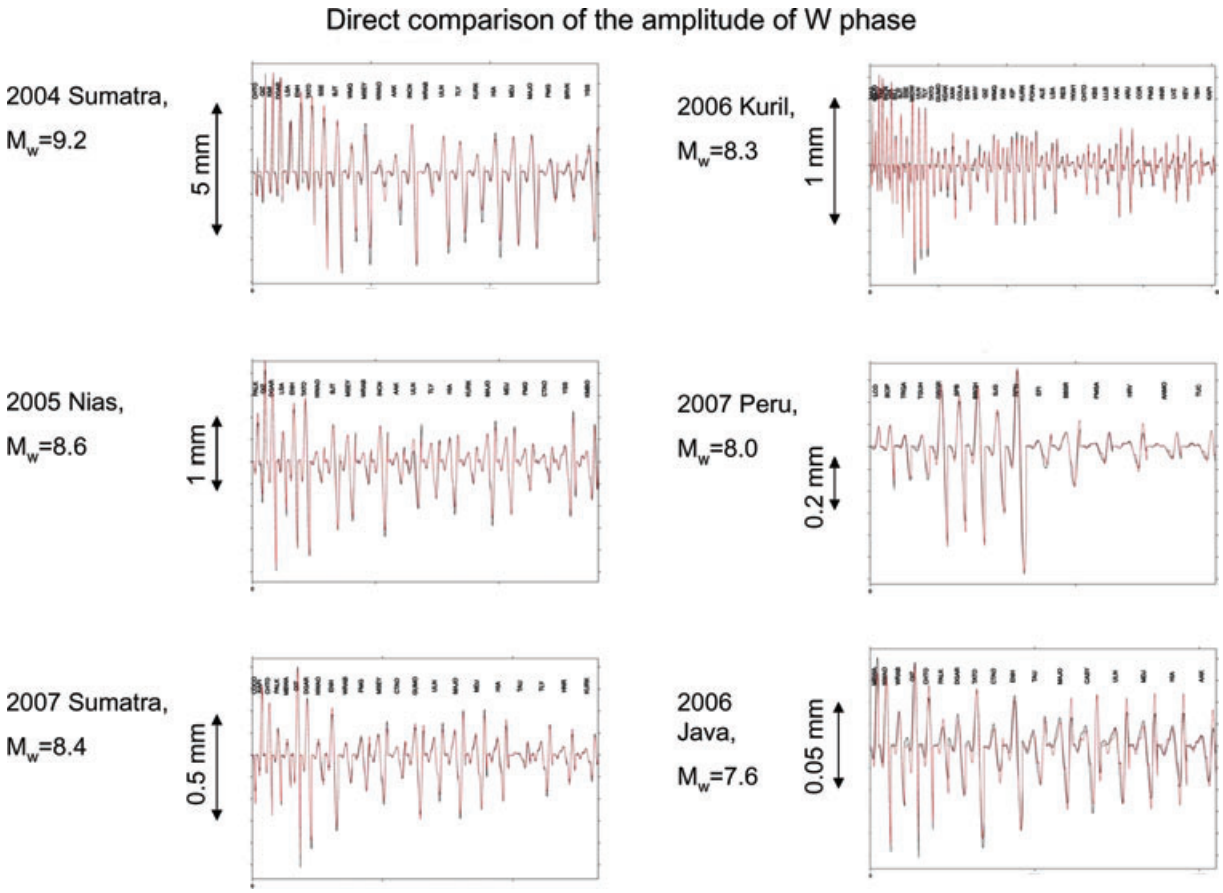

Figure 18. Direct comparison of the W-phase amplitude with the event $M_{\rm w}$. The amplitude of W phase can be used to estimate $M_{\rm w}$.

station distribution is relatively uniform, the average amplitude of the concatenated W phase can be used to estimate the approximate long-period magnitude of the event. Fig. 18 shows examples of the concatenated W phases for several events with different $M_{\rm w}$. The difference in the amplitude is obvious, which will give the operator an approximate magnitude of the event. This method is similar to the traditional magnitude determination.

We can make this approach a little more quantitative by writing the maximum of W phase amplitude, max $|u_w(\Delta_i,\ \Phi_i)|$, at a distance of Δ_i and Φ_i by

$$\max |u_w(\Delta_i,\ \Phi_i)| = q(\Delta_i)\left[a - b\cos^2(\Phi_i - \Phi_0)\right], \qquad (12)$$

where $q(\Delta)$ is the W phase distance attenuation curve, and $\left[a - b\cos^2(\Phi_i - \Phi_0)\right]$ is the azimuthal variation of W phase amplitude. $q(\Delta)$ is normalized to unity at a reference distance of 30°. We established the amplitude attenuation curve using the synthetic waveforms as shown in Table 1. The form of the azimuthal variation given above is taken from the typical pattern for a thrust earthquake (e.g. Kanamori 1970; Kanamori & Given 1981, 1982). Strictly speaking, the amplitude attenuation curve depends on the azimuth and the depth of the event, and the azimuthal pattern depends on the source mechanism. However, for purposes of the preliminary determination of the event magnitude, this simple expression should be adequate. We can determine a, b and Φ_0 from the observed W phase amplitude in the least-squares sense. Fig. 19 plots the relation between $M_{\rm w}$ and the average amplitude $a - b/2$ determined for the events with various $M_{\rm w}$. Despite the considerable scatter, we can estimate $M_{\rm w}$ from the observed W phase amplitudes before performing W phase inversion. This preliminary estimate of $M_{\rm w}$ can be used as the initial estimate of the time delay, t_d, to be used for inversion.

What is described above is not essential for WP inversion, but we believe that it is useful for enhancing the robustness and speed of seismic tsunami warning using W phases, and is recommended as part of implementation of the method for practical purposes.

9 CONCLUSION

W phase can be extracted by point-by-point time domain deconvolution of broad-band seismograms. This method would allow easy and robust real-time monitoring of tsunamigenic potential of earthquakes and inversion of W phase for the determination of $M_{\rm w}$ and the source mechanism. Because of the fast group velocity of W phases, all the data required for inversion can be collected within 15–30 min after the origin time of the earthquake. With pre-computed Green's functions, computation time for inversion is insignificant compared with the time required for data collection and processing. When broad-band seismograms are available at regional distances (i.e. $\Delta \leq 10°$), we can determine satisfactory solutions with the present method within 6 min after the origin time.

Since the propagation of W phase is not strongly affected by the Earth's structural heterogeneity caused mainly by oceans and continents, the signals from large earthquakes are usually clean and can be matched well by synthetic waveforms. Thus, inversion of W phases provides additional information on the source to that obtained from the traditional body- and surface wave studies.

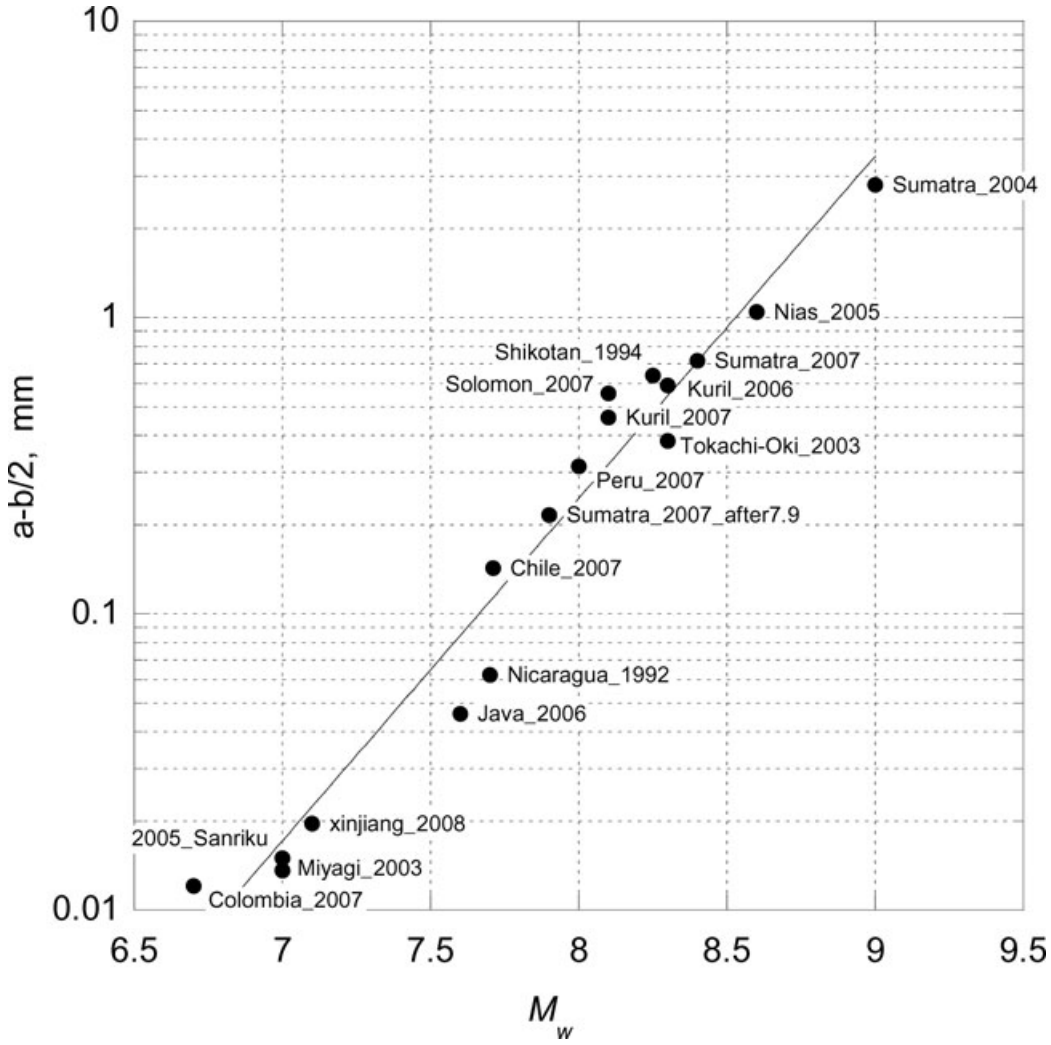

Figure 19. The average amplitude (a–b/2) of W phase and M_w from which an initial guess of M_w can be made.

Table 2. Distance attenuation relation for W phase normalized at $\Delta = 30^\circ$.

Δ (°)	q (Δ)
10.0	1.4
20.0	1.2
30.0	1.0
40.0	0.70
50.0	0.56
60.0	0.61
70.0	0.56
80.0	0.50
90.0	0.52

W phase arrives before the large amplitude surface waves and is always on scale even if the surface waves clip the record. Clipping of seismograms for very large earthquakes has been a serious problem for very large earthquakes like the 2004 Sumatra–Andaman Is. earthquake and the use of W phase would significantly increase the utility of global networks.

ACKNOWLEDGMENTS

We thank Göran Ekström and an anonymous reviewer for helpful comments on the original manuscript, and Rhett Butler for helpful technical discussion on global seismic network data. This work made use of GMT and SAC software and Federation of Digital Seismic Networks (FDSN) seismic data. The Incorporated Research Institutions for Seismology (IRIS) Data Management System (DMS) was used to access the data.

REFERENCES

Ammon, C.J. *et al.*, 2005. Rupture process of the 2004 Sumatra-Andaman earthquake, *Science*, **308**, 1133–1139.

Dziewonski, A.M. & Anderson, D.L., 1981. Preliminary Reference Earth Model (PREM), *Phys. Earth planet. Inter.*, **25**, 297–356.

Dziewonski, A.M., Chou, T.-A. & Woodhouse, J.H., 1981. Determination of earthquake source parameters from waveform data for studies of global and regional seismicity, *J. geophys. Res.*, **86**, 2825–2852.

Ekström, G., Dziewonski, A.M., Maternovskaya N.N. & Nettles, M., 2005. Global seismicity of 2003: centroid-moment-tensor solutions for 1087 earthquakes, *Phys. Earth planet. Inter.*, **148**(1–2), 327–351.

Global CMT catalog; GCMT. http://www.globalcmt.org.

Gilbert, F., 1970. Excitation of the normal modes of the Earth by earthquake sources, *Geophys. J. Roy. Astron. Soc.*, **22**, 223–226.

Harvard CMT catalog; http://www.seismology.harvard.edu/CMTsearch.html.

Hirshorn, B. & Weinstein, S., 2008. Rapid estimates of earthquake source parameters for tsunami warning: the example of the Pacific Tsunami Warning Center, in *Encyclopedia of Complexity and Systems Science*, ed. Lee, W.H.K., Springer, in press.

Kanamori, H., 1970. Synthesis of long-period surface waves and its application to earthquake source studies—Kurile Islands earthquake of October 13, 1963, *J. geophys. Res.*, **75**, 5011–5027.

Kanamori, H., 1993. W phase, *Geophys. Res. Lett.*, **20**(16), 1691–1694.

Kanamori, H. & Given, J.W., 1981. Use of long-period surface waves for rapid determination of earthquake source parameters, *Phys. Earth planet. Inter.*, **27**, 8–31.

Kanamori, H. & Given, J.W., 1982. Use of long-period surface waves for fast determination of earthquake source parameters; 2. Preliminary determination of source mechanism of large earthquakes (Ms $>=$ 6.5) in 1980, *Phys. Earth planet. Inter.*, **30**, 161–172.

Kanamori, H., Maechling, P. & Hauksson, E., 1999. Continuous monitoring of ground motion parameters, *Bull. seism. So. Am.*, **89**, 311–316.

SAC, Seismic analysis code; http://www.iris.edu/manuals/sac/manual.html.

Saito, M., 1967. Excitation of free oscillations and surface waves by a point source in a vertical heterogeneous Earth, *J. geophys. Res.*, **72**, 3689–3699.

Satake, K., 2007. Tsunamis, in *Treatise on Geophysics*, **Vol. 4**, ed. Kanamori, H., Elsevier, Amsterdam.

Satô, Y. & Usami, T., 1962. Basic study on the oscillation of a homogeneous elastic sphere III. Boundary conditions and the generation of elastic waves, *Geophys. Mag.* **31**, 49–62.

Takeuchi, H. & Saito, M., 1972. Seismic surface waves, in *Methods in Computational Physics*, Vol. 11, pp. 217–295, ed. Bolt, B.A., Academic Press, New York.

Wielandt, E. & Streckeisen, G., 1982. The leaf-spring seismometer: design and performance, *Bull. seism. Soc. Am.*, **72**(6), 2349–2367.

Zhu, L., 2003. Recovering permanent displacements from seismic records of the June 9, 1994 Bolivia deep earthquake, *Geophys. Res. Lett.*, **30**, 14, doi:10.1029/2003GL017302.

APPENDIX: CLIPPING OF GLOBAL BROAD-BAND RECORDS FOR THE 2004 SUMATRA–ANDAMAN IS. EARTHQUAKE

For the 2004 Sumatra–Andaman Is. earthquake ($M_w = 9.2$), all the global broad-band records at $\Delta \leq 41^\circ$ we looked at (15 stations) were clipped or became non-linear as shown in Fig. A1. These records are not useable for the standard analysis in which the conventional frequency-domain process is used. However, W phase could be retrieved with time-domain deconvolution from the records of 13 out of the 15 stations. Also, with the traditional frequency-domain analysis, it is often difficult to see where clipping or non-linear response started happening. With the time-domain analysis, it is obvious as shown in Fig. A1.

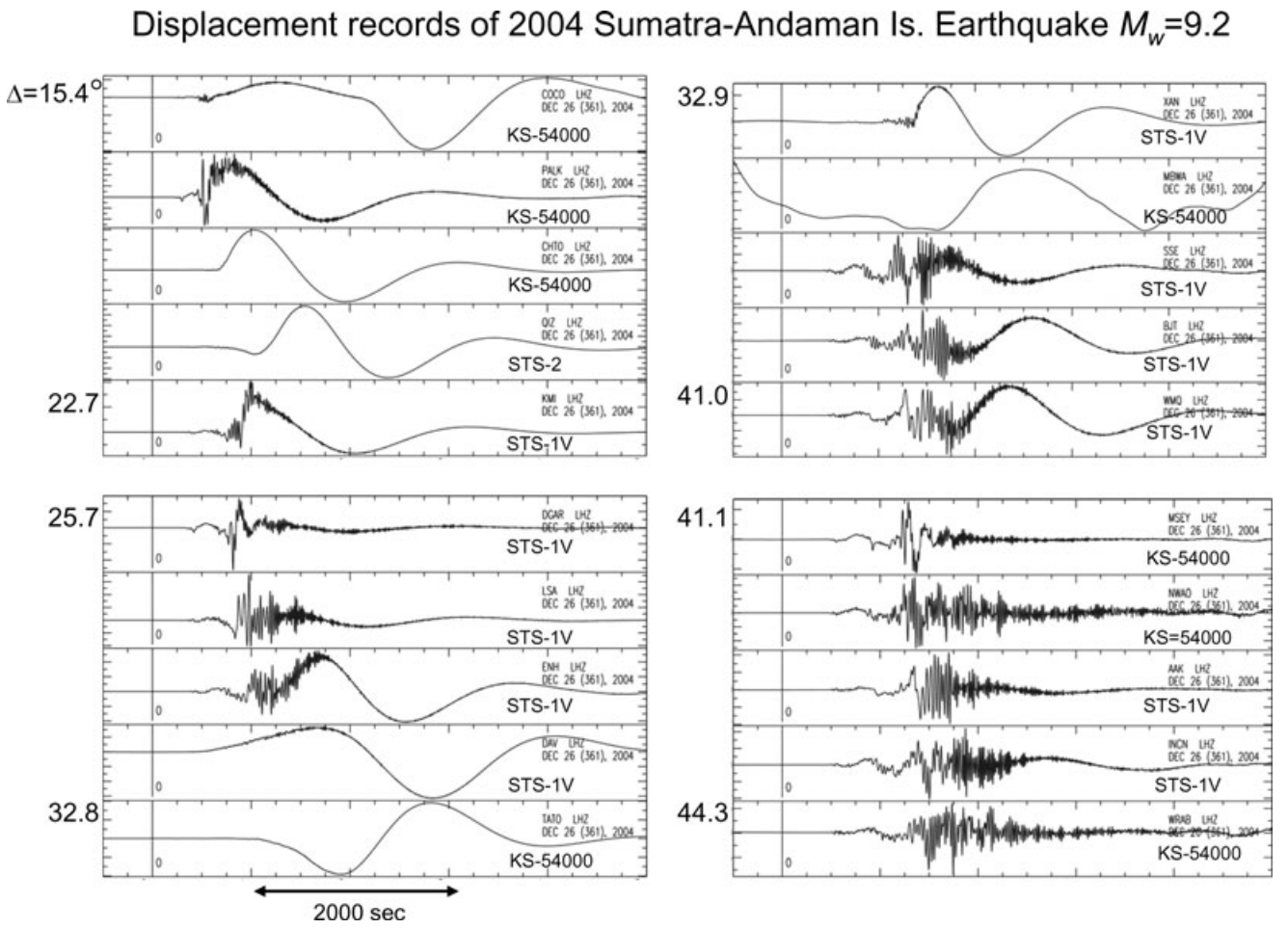

Figure A1. Displacement records of the 2004 Sumatra–Andaman Is. earthquake obtained with time-domain deconvolution of the original broad-band records.